Search for Supersymmetry with Gauge-Mediated Breaking in Displaced Photon Events using ECAL Timing and Missing Transverse Energy in PP Collisions at $\sqrt{S} = 8$ TeV

Tambe Ebai Norbert

January 30, 2014

Abstract

Particles with long lifetime also known as long lived particles are predicted to exist in nature by some models beyond the SM. GMSB model is an example of such a model. It predicts the Neutralino($\tilde{\chi}_1^0$) being the NLSP to decay into a LSP-the gravitino ($\tilde{G}$) and a photon (γ). The photon because of the neutralino long life time will arrive late at the detector while the weakly interacting gravitino will emerge as an imbalance in the transverse momenta of all the reconstructed particles in an event. In this article, we propose a search for neutralino produced in $\sqrt{S} = 8$ TeV proton-proton collisions through its decay into a photon and a gravitino. The photon time is measured using the ECAL while the imbalance in transverse momentum also known as $\vec{E}_{\mathrm{T}}^{\mathrm{miss}}$ calculated from transverse momentum measurement using the tracker, ECAL and the HCAL of the CMS detector is used to infer the presence of the gravitino.

1 Introduction

Supersymmetry (SUSY) is believed to be a symmetry in nature between bosons -integer spin and fermions -half integer spin particles. It is an extension of the standard model (SM) predicting the existence of massive neutrally charged particles that can often decay into a photon and a stable weakly interacting particle. The long life time of these particles implies most of them will travel a few distance from their point of production before decaying inside the detector. As a result, most of the photons produced through their decay will not emerge from the point of production of these particles as normal (SM) photons will but rather from a secondary position. Such photons will arrive late at the Electromagnetic calorimeter (ECAL) pointing off the crystal's major axis at the arrival point compared to most normal photons originating from the production point. They are said to be "Off-Pointing" (OP) or "Displaced Photons" (DP). Meanwhile the stable weakly interacting particle will travel through the detector undetected. Its presence however can be infered using the imbalance in transverse momenta calculated from the total transverse momentum of all the reconstructed particles in a event. This imbalance in transverse momenta is also known as the missing transverse momentum $\vec{E}_{\mathrm{T}}^{\mathrm{miss}}$. The presence of a DP and a weakly interacting particle will give a unique topological signal not resulting from known interactions currently described by the SM. Thus using the ECAL to mearsure the time of arrival of these photons which they are supposed to arrive late because of their displaced vertices and calculating correctly the $E_{\mathrm{T}}^{\mathrm{miss}}$ in each event might indicate the presence of new physics (NP). This note presents the main features of the search for DP and gravitino using the CMS detector. It is organized as follows: In section 1, we give a theoretical motivation of a phenomenological model describing the neutralino production and decay while section 2 contains a description of the subdetectors in the CMS detector useful in our search: the tracker, the electromagnetic and hadronic calorimeters. A brief analysis strategy is given in section 3, including some important variables we hope will be useful in separating background from signal and ending with our current work on the analysis. Our conclusion is in section 4 of this article.

1.1 Theory

There are lots of published articles explaining the different ways in which Supersymmetry (SUSY) is spontaneously broken. A popular understanding of spontaneously broken SUSY is that the Vacuum Expectation Value (VEV) of an auxiliary field F which is neccessary for maintaining this symmetry (SUSY) up to the quantum level (Off-Shell) suddenly becomes non-zero. However, at our present easily accessible energy scales through accelerators testing models like SM, we do not observe such a symetry between bosons and fermions. Thus a common speculation is

that SUSY breaking cannot occur at energy scales close to SM or supersymmetric extensions of SM such as the Minimal Supersymmetric Standard Model (MSSM). One of the consequences of such an occurrence will be the existence of supersymmetric particles with their masses smaller than those of the already observed SM particles. Since we are yet to observe such particles from current experiments at the electro-weak energy scale with mass less than 173 GeV [11], it is likely that SUSY breaking if possible must happen at some higher energy scale or early universe period probably in some set of fields entirely not connected to the fields in the MSSM. These set of fields are usually refered to as the *"Hidden Sector"* in some SUSY breaking models. The communication or mediation of SUSY breaking from this high (thousands or millions of TeV) energy scale down to our MSSM energy scales (few TeV) can be done through gravitational, gauge interactions or anomaly in the topology. SUSY breaking models are developed based on any 1,2 or all 3 of these interactions depending on certain phenomenology observations to be explained.
In this article, we focus on Gauge Mediated Supersymmetry Breaking (GMSB) models as these are both theoretically and experimentally motivating.

1.1.1 Motivation

A first motivation for GMSB model is that, among many SUSY models build with constraints from cosmology, for example, the constraint that any SUSY model should give rise to an acceptable dark matter density between $0.1 \leq \Omega_\chi \mathrm{h}^2 \leq 0.3$ as observed in [2], it predicts that the gravitino is a candidate particle for cold dark matter with its contribution to this density given as $\Omega_{\frac{3}{2}}\mathrm{h}^2 = \dfrac{m_{3/2}}{\mathrm{keV}}\left[\dfrac{100}{g_*(T_f)}\right]$ [3]. $m_{\frac{3}{2}}$ is the mass of the gravitino and $g_*(T_f)$ is a function quantifying the effective degrees of freedom of the gravitino at T_f (being the temperature of the early universe when its contribution remains constant with respect to the rate of expansion of the universe). This degree of freedom is usually between 100 to 200 in SUSY models. h is known in cosmology as the Hubble constant given in units of 100 $\mathrm{kmsec}^{-1}\mathrm{Mpc}^{-1}$.
A second motivation for GMSB models comes from comparing theoretical prediction to experimental low energy measurements of the anomalous magnetic moment of the muon. Measurements made by the Muon $g_\mu - 2$ collaboration in [4] compared to SM predictions in [5] suggest that $a_\mu = \frac{g_\mu - 2}{2}$, up to theoretically as well as experimentally understood uncertainties must lie within $-6 \times 10^{-10} < a_\mu < 58 \times 10^{-10}$. This range of uncertainty in the agreement between experiment and SM prediction paves the way for any would-be disagreement to be interpreted as the existence of SUSY particles contributing to the SM prediction given in GMSB models as $\delta a_\mu \simeq 15 \times 10^{-10} (\frac{100GeV}{\tilde{m}})^2 \tan\beta$. $\tilde{m}$ is the typical mass scale of weakly interacting SUSY particle and $\tan\beta$ is a free parameter of the theory. Other low energy measurments like the branching ratio of the rare decay of B-messons (in parton level given as $b \to s\gamma$) as found by the CLEO collaboration [6] to be within a range $2 \times 10^{-4} < \mathrm{BR}(b \to s\gamma) < 4.15 \times 10^{-4}$ compared with results from prediction in GMSB suggest the existence of SUSY particles contributing to this decay rate.
Meanwhile, from a theoretical position, GMSB models are particularly interesting because they make predictions of decay rates and cross sections which do not lead to excesses in Flavor Changing Neutral Currents (FCNC) which is yet to be observed experimentally in such large quantities as predicted by other SUSY breaking models such as constraint MSSM (mSUGRA). They are the closest among all other SUSY breaking models to providing direct understanding to why the Plank energy scale ($M_p = 10^{19}$ GeV) is very different from the Electro-Weak energy scale ($E_{EWK} \approx 100$ GeV).

1.2 Phenomenology

GMSB models consist of two main sectors. The *observable sector* containing the quarks, leptons and the two Higgs doublets, together with their super-symmetric partners (MSSM) and the *hidden sector* which is responsible for SUSY breaking.
This breaking must occur in such a way that its effect is felt at the TeV energy scale. Such a SUSY breaking is termed soft breaking which technically means most of the terms in the SUSUY breaking langragian must consist mostly of dimensionful couplings such that the mass scale cannot exceed the TeV region. It is these soft terms which provide mass to all of the SUSY partners of the known SM particles.
Analoguos to the Electroweak symmetry breaking where gauge and Yukawa interactions communicate the Electroweak symmetry breaking to the SM particle states, in SUSY breaking the original SUSY breaking is also communicated to the ordinary particle supermultiplets. However, the only difference is that because of the supertraced theorem, one cannot construct SUSY breaking models where SUSY breaking is communicated to ordinary supermultiplets through tree level renormalisable couplings as in the Electroweak breaking scenario. Nevertheless, in

the same way as in SM in which the Higgs vacuum expectation value (VEV) determines the electroweak symmetry breaking so too in constructing realistic SUSY models we require a chiral superfield X to acquire a VEV and hence determine the scale of SUSY breaking. X must acquire a VEV along its scaler and auxiliary components as

$$\langle \mathrm{X} \rangle = \mathrm{M} + \theta^2 \mathrm{F} \tag{1}$$

where θ is a Grassman number. This analoguos Higgs sector in SM is what is refered to as the hidden or sometimes secluded sector and has no renormalisable tree level couplings to the "observable sector" containing ordinary SM and SUSY particles.
The simplest structure of this secluded sector is the scenario is which the goldstino superfield is X and couples at tree level to a "messenger sector" formed by some new superfields which transform under a gauge group as a real non-trivial representation. This tree level coupling generates a supersymmetric mass of the order of M (one of the main fundamental parameters of any GMSB model) for the mass of this messenger field and a mass squared splittings inside the messenger supermultiplets of the order of F (another fundamental parameter). M and F are parameters which can vary from a few TeV to the Plank energy scale.

In a Minimal Supersymmetric Standard Model(MSSM), the messenger sector is described by N_f flavors of chiral superfields $\mathbf{\Phi_i}$ and $\bar{\mathbf{\Phi}}_\mathbf{i}$ $(i = 1, \cdots, \mathrm{N}_f)$. The interaction between the chiral messenger superfields Φ and $\bar{\Phi}$ and the goldstino superfield X is given by the superpotential terms

$$\mathrm{W} \;=\; \lambda_{ij} \bar{\Phi}_i \mathrm{X} \Phi_j \tag{2}$$

If we replace in eq.(2) the X VEV, see eq.(1), we find that the spinor components of Φ and $\bar{\Phi}$ form Dirac fermions with masses λM, while the scalar components have a squared mass matrix which when diagonalised and solved gives squared masses of the messenger fields as $\mathrm{M}^2 \pm \mathrm{F}$ [3], where the mass scale, $\sqrt{\mathrm{F}}$, is the measure of supersymmetry breaking in the messenger sector.
The messenger fields couple to the observable sector in a way that unification of couplings is preserved and by gauge invanriance the masses of vector bosons and fermions is also preserved. Splitting arises at quantum level because of gauge interactions between fields in the observable sector and messenger fields. The main assumption here is, the positivity of the messenger squared mass which requires $\mathrm{F} < \mathrm{M}^2$. In fact the most realistic case is to assume $\mathrm{F} \ll \mathrm{M}^2$. This assumption makes it possible that in an effective field theory below the messenger scale M, super-symmetry breaking can be treated as a small effect. The procedure is as follows: starting from an effective field theory valid for mass scale M and integrating out all heavy messenger fields, we can solve the renormalization-group(RG) equations in the exact SUSY theory. At the end, we replace X with the VEV, to obtain physical mass spectrum for the soft terms to find the mass difference between the SUSY particles and the SM particles is within the TeV energy scale. [3].
One very important feature of the gauge-mediated mass spectrum is flavor universality meaning, the messenger fields interact with all particles with different flavor or different generation in the same way which is a consequence of the symmetry of gauge interactions. If we require that gravity-mediated contributions are small, say one per mill of the soft squared masses so as not to break the flavor universality, then gravity generates soft terms with typical size $\mathrm{F}/\mathrm{M_P}$. This gives a rough upper bound on the messenger scale

$$\mathrm{M} \;\leq\; \frac{1}{10^{\frac{3}{2}}} \frac{\alpha}{4\pi} \mathrm{M_P} \sim 10^{15}\ GeV \tag{3}$$

where $\mathrm{M_P} = (8\pi \mathrm{G_N})^{-1/2} = 2.4 \times 10^{18} GeV$ is the reduced Planck mass. However, there are other models which indicate upper bound on messenger scale of $\mathrm{M} \leq 10^{13}\ GeV$.

1.2.1 Gravitino as LSP

Spontaneous super-symmetry breaking produces a physical spectrum containing a massless spin-1/2 fermion called the goldstino. Coupling the globally super-symmetric theory to gravity produces a locally super-symmetric theory in which the goldstino provides the longitudinal modes of the spin-3/2 partner of the graviton, the gravitino. The result of this superhiggs mechanisms is that, the gravitino acquires a super-symmetry-breaking mass which, under the condition of vanishing cosmological constant, is given by

$$m_{\frac{3}{2}} \;=\; \frac{F_0}{\sqrt{3}\mathrm{M_P}} \tag{4}$$

F_0 is the total contribution of the super-symmetry-breaking VEV of the auxiliary fields, normalized such that the vacuum energy of the globally SUSY theory is $\mathrm{V} = \mathrm{F}_0^2$. F_0 is not the same as F which appears in the sparticle masses

through $\Lambda = \frac{\mathrm{F}}{\mathrm{M}}$. In fact, F_0 is the fundamental scale of super-symmetry breaking, F is the scale of super-symmetry-breaking felt by the messenger particles, i.e. the mass splitting inside their supermultiplets. We define the ratio $k \equiv \frac{\mathrm{F}}{\mathrm{F}_0}$ which depends on how super-symmetry breaking is communicated to the messengers. If the communication occurs via direct interaction, then this ratio is just given by a constant parameter like the parameter λ in eq.(2) above. The communication can also occur radiatively in which case k is smaller than 1 as oppose to 1 for direct interactions. We rewrite the gravitino mass as

$$m_{\frac{3}{2}} = \frac{\mathrm{F}}{k\sqrt{3}\mathrm{M_P}} = \frac{1}{k}\left(\frac{\sqrt{\mathrm{F}}}{100TeV}\right)^2 2.4\ eV, \tag{5}$$

where the model-dependent coefficient k is such that $k < 1$, and possibly $k \ll 1$. $m_{\frac{3}{2}}$ is exactly a measure of gravity-mediated effects. It is indeed the solution to the flavor problem in gauge mediation with its effect much smaller than gauge-mediated contributions. This implies, the gravitino is stable and the LSP.
Assuming conservation of R-parity, (where R-parity is defined as $P_R = (-1)^{3(B-L)+2S}$ with B and L being baryon and lepton numbers respectively, and S is spin) supersymmetric particles(sparticles) decay in cascade that leads to gravitino. Which means, single sparticles cannot decay into SM particles alone and superpartners must be produced in pairs from SM particles.
To compute the decay rates for neutralino, we need to know the interaction Lagrangian at lowest order in the gravitino field. With $\sqrt{\mathrm{F}} \ll \mathrm{M_P}$, the dominant gravitino interactions come from its spin-1/2 component, the interaction Lagrangian can be computed in the limit of global super-symmetry. In the presence of spontaneous super-symmetry breaking, the super current J^μ_Q satisfies the equation

$$\partial_\mu J^\mu_Q = -\mathrm{F}_0 \gamma^\mu \partial_\mu \tilde{G}, \tag{6}$$

This is the goldstino equation of motion. The corresponding interaction Lagrangian is

$$\mathcal{L} = -\frac{1}{\mathrm{F}_0} J^\mu_Q \partial_\mu \tilde{G}. \tag{7}$$

The goldstino couples to bilinear, meaning we replace J^μ_Q in eq.(7) by its expression for free fields and obtain

$$\mathcal{L} = -\frac{k}{\mathrm{F}}\left(\bar{\psi}_L \gamma^\mu \gamma^\nu \partial_\nu \phi - \frac{i}{4\sqrt{2}} \bar{\lambda}^a \gamma^\mu \sigma^{\nu\rho} \mathcal{F}^a_{\nu\rho}\right) \partial_\mu \tilde{G} + h.c. \tag{8}$$

where ϕ and ψ are the scaler and fermion components of a generic chiral multiplet and λ^a and $\mathcal{F}^a_{\mu\nu}$ are the Majorana spinor and gauge field strength belonging to a vector super-multiplet.

For on-shell particles, by using the equation of motion, the golstino Lagrangian in eq.(8) can be written as a Yukawa interaction with the chiral superfields and magnetic moment-like interaction with gauge particles,

$$\mathcal{L} = \frac{k}{\mathrm{F}}\left[\left(m^2_\psi - m^2_\phi\right) \bar{\psi}_L \phi + \frac{\mathrm{M}_\lambda}{4\sqrt{2}} \bar{\lambda}^a \sigma^{\nu\rho} \mathcal{F}^a_{\nu\rho}\right] \tilde{G} + h.c. \tag{9}$$

Both goldstino interactions are proportional to the mass splitting inside the super-multiplet and inversely proportional to the scale of super-symmetry breaking. The next-to-lightest super-symmetry particle(NLSP) plays an important role the phenomenology of gauge mediation. Assuming R-Parity conservation, we expect that all sparticles will promptly decay into cascades leading to the NLSP, with the NLSP then decaying into the gravitino via 1/F interactions. Therefore, the nature of NLSP determines the signatures in collider experiments. The possibility of NLSP being a neutralino seems interesting because of its dominant B-ino component (from mass spectra), for moderate M, N and Λ. In fact the SUSY benchmark point SPS 8 in [8] uses the following parameters $\Lambda = 100$ TeV, $\mathrm{M}_{mes} = 200$ TeV, $\mathrm{N}_{mes} = 1$, $\tan\beta = 15$, and $\mu > 0$. The neutralino decay rate is calculated as

$$\Gamma\left(\tilde{\chi}^0_1 \to \gamma \tilde{G}\right) = \frac{k^2 \kappa_\gamma m^5_{\tilde{\chi}^0_1}}{16\pi \mathrm{F}^2} = k^2 \kappa_\gamma \left(\frac{m_{\tilde{\chi}^0_1}}{100GeV}\right)^5 \left(\frac{100TeV}{\sqrt{\mathrm{F}}}\right)^4 2 \times 10^{-3}\ eV, \tag{10}$$

κ_γ is a constant parameter depending on the components of $\tilde{\chi}^0_1$. This is the most dominant decay mode. To be able to understand this signal at colliders, we need the average distance traveled by the NLSP with mass $\tilde{m}$ and produced with energy E as

$$\mathsf{L} = \frac{1}{\kappa_\gamma}\left(\frac{100GeV}{\tilde{m}}\right)^5 \left(\frac{\sqrt{\frac{\mathrm{F}}{k}}}{100TeV}\right)^4 \sqrt{\frac{E^2}{\tilde{m}^2} - 1} \times 10^{-2}\ cm \tag{11}$$

Depending on the value of $\sqrt{\frac{F}{k}}$, the NLSP can either decay within microscopic distances or decay well outside the solar system.

If $\sqrt{\frac{F}{k}}$ is large(roughly greater than 10^6 GeV), the NLSP decays outside of the detector and behaves like a stable particle and the neutralino signature resembles those of the ordinary super-symmetric scenarios with stable neutralino.

For small $\sqrt{\frac{F}{k}}$ (typically $\leq 10^6$ GeV) the NLSP promptly decays and the experimental signature is given by events with missing transverse energy, imbalance in the final-state momenta and a pair of photons.

In the intermediate region between the two regions for $\sqrt{\frac{F}{k}}$, things become very much interesting. Here the NLSP decay length could be measurable as a vertex displacement of the final-state photon. This is experimentally interesting or favorable, because it allows a better background rejection. It is also theoretically interesting, because the measurement of the decay length gives direct information on the value of $\sqrt{\frac{F}{k}}$. This has additional advantage, since other measurements are mainly sensitive only to the mass scale $\Lambda = \frac{F}{M}$ which roughly determines the mass spectrum. In fact on-going analysis is being carried out to measure and set limits on the NLSP decay length.

1.3 Previous Limits

Neutralino search at both electron and hadronic colliders have previously been performed. A search analysis at LEP, a lepton-lepton collider, searching for diphoton plus missing energy events resulted to a combined 95 % CL limit on the cross section, $\sigma\left(e^+e^- \to \tilde{\chi}_1^0\tilde{\chi}_1^0\right) \times BR\left(\tilde{\chi}_1^0 \to \gamma\tilde{G}\right)$ at $\sqrt{S} = 172$ GeV of about $\sigma_{\tilde{\chi}_1^0} < 0.3$ pb for $m_{\tilde{\chi}_1^0} < 70\ GeV/c^2$ and $\sigma_{\tilde{\chi}_1^0} < 0.15$ pb for 70 GeV/c^2 $< m_{\tilde{\chi}_1^0} < 85$ GeV/c^2 for neutralino with decay length within $0.1 < c\tau < 50$ cm. In a fairly parameter independent way, $m_{\tilde{\chi}_1^0} < 73$ GeV/c^2 are excluded as long as $\tilde{\chi}_1^0$ decays occur inside the detector [9].

For a hadron collider experiment, CDF and DØ, at Tevatron, searched for diphoton events with large missing energy during which the measured missing energy distribution were found to be in agreement with SM background. DØ set a bound on the cross section $\sigma(p\overline{p} \to \gamma\gamma E_{\mathrm{T}}^{\mathrm{miss}} + X) < 185$ fb at 95 % CL corresponding to excluding neutralinos lighter than 70 GeV/c^2 in decay channel $\tilde{\chi}_1^0 \to \gamma\tilde{G}$ with decay length $0.1 < c\tau < 100$ cm [10]. In run II of Tevetron, CDFII observed no candidate events in a similar diphoton events with large missing energy in $2.6 \pm 0.2\ \ fb^{-1}$ of $p\overline{p}$ collisions at$\sqrt{S} = 1.96$ TeV. This resulted in a limit of $m_{\tilde{\chi}_1^0} > 149\ GeV/c^2$ with lifetimes; $\tau_{\tilde{\chi}_1^0} \ll 1$ ns completely excluding neutralinos with lifetime; $\tau_{\tilde{\chi}_1^0} \leq 2$ ns. Recently, ATLAS did a similar diphoton search which resulted to a limit of $\sigma < (22 - 129)$ fb in the context of generalised GMSB with a bino-like neutralino [11]. Another group within the CMS collaborators is currently working on a similar analysis [12].

From the above results, it indicates that any search for neutralino in the decay channel of a photon and gravitino, must be in the region where the neutralino mass is well above 150 GeV/c^2 with a lifetime $\tau_{\tilde{\chi}_1^0} \geq 2$ ns. The ECAL detector has a radial length of ≈ 1.5 m corresponding to a lifetime of ≈ 5 ns. Thus if one performs a search for slowly moving neutralinos produced at the LHC, it is clear that there is still enough room to improve on these limits.

2 CMS Detector

The main feature of the Compact Muon Solenoid (CMS) apparatus is a superconducting solenoid of 6 m internal diameter providing a field of 3.8 T neccessary for good momentun resolution. This field encloses the silicon pixel and strip tracker, the crystal electromagnetic calorimeter (ECAL) and the brass/scintillator hadron calorimeter (HCAL). Very long lived particles like muons are measured in gas-ionization detectors embedded in the steel return yoke located at the outermost section of the detector. It has a simple structure consisting of the barrel and endcap detectors and an extensive forward calorimetry. The CMS apparatus has an overall length of 22 m, a diameter of 15 m, and weighs 14 000 tonnes.

2.1 ECAL, HCAL and Tracker

Calorimeters have a unique property of improving relative energy resolution with increasing energy thus making them indispencable in high energy physics experiments. In the decay of neutralino, we espect the photon produced to have a very high energy(above 90GeV) and the gravitino which is weakly interacting to emerge as large missing energy. Therefore it is imperative to describe how the calorimetry system of CMS is designed to ensure that we

can detect these photons. We also provide a brief description of the tracking system use for calculating missing transverse energy.

2.1.1 ECAL

The Ecal consists of the Barrel(EB) region occupying a pseudo-rapidity of $|\eta| < 1.479$ and two Endcaps (EE) regions covering $1.479 < |\eta| < 3.0$. Sitting right in front of the EE, is a Preshower(ES) detector made of silicon strip sensors interleaved by lead making it a few radiation length thick. Its main purpose is to improve in γ/π^0 descrimination in the EE regions.

The EB and EE combined consist of 75848 lead tungstate ($PbWO_4$) scintinlating crystals. At the longitudinal end of each crystal is coupled two Avalanche-Photodiodes(APDs) for EB crystals and Vacuum-Phototriodes(VPTs) for EE crystals for scintilating light collection developed in the crystals. VPTs are used for EE crystals because of their better resistance against high radiation. This large number of crystals provide an almost 4π coverage of solid angle which is important for missing energy calculation.
$PbWO_4$ has a radiation length (X_0) of $\simeq 0.89$ cm. The total longitudinal length of a crystal in EB is $25.8X_0$ and $24.7X_0$ in EE providing enough absorber thickness for most of the energy of the incident very energetic photon or electron to completely lose through a cascade process in the crystal. This energy loss is mainly through radiation of photons(*Bremsstrahlung*) and pair production. The "amplitude" or "probability" of these processes is proportional to the nuclear charge or number of electrons, Z of the material. $PbWO_4$ is a high Z material which makes it a good choice along with other properties like fast scintilation time for ECAL calorimetry. Low energy electrons lose their energy through other processes like ionization and excitation. Eventhough $PbWO_4$ is a heavy material, Compton scattering and photoelectric effect is still possible as most of the photons with energy below a few MeV have their dominant contribution to energy loss from mainly these processes.
$PbWO_4$ crystals also have a Moliere radius of 2.4 cm. This ensures that on average about 95 % of the electromagnetic shower energy is contained within the crystal volume therefore reducing the transverse spread of the electromagnetic cascade arising from multiple scattering of electrons. It improves on the estimation of the transverse position of impact of the incident particle. This Moliere radius implies $PbWO_4$ is very dense and compact therefore resistant to radiation making it suitable for a high radiation environment like the LHC.
The crystals are tapered and arranged in a projective goometry pointing $\approx 3^o$ away from the mean beam collision point. The purpose of this is to minimize inter crystal gaps hence preventing photons or part of the photon cluster from going through these gaps undetected. This improves the energy calibration and reduces the contribution to the constant term in the Ecal energy resolution and is the dominant contribution for high energies and in missing energy calculations.
$PbWO_4$ has a fast(80 % of the light emitted within 25 ns) scintilation process. It peaks in the blue region (425 nm) making photo-detection simpler and reliable in a fast (bunch crossing frequency of 40 MHz) timing requirement environment like the LHC. Although the light-yield for $PbWO_4$ is rather low ($\approx$ 70photons/ MeV), the photodiodes have internal gain (50 for APDs and 10 for VPTs) and good quantum efficiency of 75 % for APDs and 20 % for VPTs of the emission wavelength. This makes it possible that signals from incident particles with energies from a few to high GeV can be recorded.

This homogenous design of the ECAL provides it with a performance which is optimal(by design) in its potential to discover a Higgs in the mass region less than 130 GeV/c^2 through the decay $H \to \gamma\gamma$. Homogenous design implies reduced noise in the detector thus better resolution since only a single material type is in use. ECAL has a current timing resolution better than 500 ps for large energy deposits(more than 10-20 GeV in the EB) [1] and an energy resolution of $\sigma/E \approx 0.45$ % for unconverted photons with energies above 100 GeV [13].

2.1.2 HCAL

Directly behind the ECAL, is the hadronic calorimeter(HCAL). Unlike the homogenous ECAL, the HCAL is an inhomogenous sampling calorimeter. The hadronic barrel(HB) and hadronic endcap(HE) of the HCAL cover a region in pseudo-rapidity of $|\eta| < 3$. The designed consist of plastic scintilating tiles with wavelength shifting fibers sandwiched between layers of brass or steel as absorber giving it a repeated interleaved structure of absorber/dead(steel or brass) and active layers of tiles of plastic scintilating material. The active material is used mainly for periodically sampling electromagnetic and hadronic components in the hadronic shower while steel and brass act as stopping material for energetic incoming hadrons in the shower. The absorber material provide fine granularity of short nuclear interaction length while tiles of plastic scintilator separates charged hadrons like protons, pions($\pi^{\pm}$),

kaons($k^{\pm}$) and neutrons from electromagnetic physics objects like photon and neutral pions contained in the incident hadronic shower. This ability to separate different components of a hadronic shower serves as the basis for some particle reconstruction algorithms making the HCAL very usefull in the reconstruction of complex physics objects like jets which usually consist of hadronic as well as electromagnetic showers. The HCAL is thus very important in missing energy calculation. Quartz fibers for Cerenkov light production placed in a steal mix occupy $3 < |\eta| < 5$. This inhomogenous design gives the HCAL, an energy resolution of $\Delta E/E \approx 0.5/\sqrt{E(GeV)}$ above 250 GeV [13].

The HCAL calorimeter is a sampling calorimeter which means it finds the particle's position, energy and arrival time by using the alternating layers of "absorber" and fluorescent "scintilating" materials which produce a rapid light pulse when a particle passes through. Some special optic fibres collect up this light and supply it to readout boxes where photodetectors amplify the signal. The amount of light in a given region is summed up over many layers of tile along the particle's path through the HCAL in depth called a "tower". The total amount of light is a measure of the particle's energy and an indicator of its type. This sampling is used to separate the hadronic and energetic electromagnetic component of the shower which passed through the ECAL unstopped.
A hadronic shower is formed when an incident hadron undergoes an inelastic collision with the nucleus of the absorber material producing secondary hadrons which as they go through successive layers of absorber material interact inelastically with other nuclei to produce further hadrons etc. The hadronic cascade loses about 30 % of incident hadron energy through nuclear excitation of the nuclei of atoms of the absorber material.
The HB calorimeter is an assembly of two half barrels each composed of 18 identical 20^o wedges in ϕ. The wedge is made of flat brass alloy absorber plate parallel to beam axis with the innermost and outermost layers made up of stainless steal interleaved by plastic scintillator tiles. The first active layer is situated directly behind the ECAL in order to actively sample low energy showering particles from the support material between the ECAL and HCAL. Each scintillator tile has a size of $\Delta\eta \times \Delta\phi = 0.087 \times\ 0.087$ and is instrumented with a single wave length shifting fiber(WLS) for better collection of light. The summed optical signals or light are converted into fast electronic signals by photosensors called hybrid photodiode(HPD).
In the foward region in η is the forward calorimeter (HF) made up of steel absorbers embedded in radiation hard quartz fibers running parallel to the beam axis and providing a fast collection of Cerenkov light. The signal results from Cerenkov light emitted in the quartz fibres embedded in the steel matrix in response to charged particles. The Cerenkov calorimeter have long and short fibers which are positioned alternatively separated by 5 mm with readouts for better sampling of the different shower components. The goal of this hardware design is to give better compensation for different shower components in the hadronic shower. The HF section enables the HCAL to pick up myriad of particles coming out of the collision region at very shallow angles relative to the beam direction.
These different sections of the HCAL in $\eta - \phi$ plane give it a unique capability to measure multi-jet events revealing the fine structure of jets. Decaying particles may produced new particles that do not leave any record of their presence in any part of the CMS detector. To spot such particles, the above HCAL sections give it an almost "hemetic" coverage making sure it captures to the extend possible every particle emerging from collisions. In this way, if we observe a particle in one side of the detector but not in the other, with imbalance of momentum and energy in the direction "transverse" to the beam direction, we can deduce that we are producing "invincible" particles. This is the primary idea in missing transverse energy calculation established as signal for very weakly interacting particles like neutrino and hopefully gravitino. Generally speaking, in the region $|\eta| < 1.74$, the HCAL cells have widths of 0.087 in pseudorapidity(η) and 0.087 rad in azimuth (ϕ). In the (η, ϕ) plane, and for $|\eta| < 1.48$, the HCAL cells map on to 5×5 ECAL crystals arrays to form calorimeter towers projecting radially outwards from close to the nominal interaction point. At larger values of $|\eta|$, the size of the towers increases and the matching ECAL arrays contain fewer crystals. Within each tower, the energy deposits in ECAL and HCAL cells are summed to define the calorimeter tower energies subsequently used to provide the energy and direction of hadronic jets.

2.1.3 Tracker

Unlike calorimeters, the tracker is basically a magnetic spectrometer where the momentum resolution is linearly proportional to the particle's momentum in a given magnetic field. This means very low momentum particles have better momentum resolution than their high momentum counterparts. The momentum of a charged particle is inversely proportional to the curvature of its trajectory in the magnetic field. By reconstructing the trajectory of the particle as it moves in the tracker; through "hits" made at various positions, we are able to deduce its curvature and hence determine its momentum. High momentum particles are less curved by the magnetic field than low momentum particles. Thus, the tracker is expected to have a very good momentum resolution for low momentum particles. The strong magnetic field and high granularity of the CMS silicon tracker allows promptly produced charged particles with $p_{\mathrm{T}} = 100 GeV/c$ to be reconstructed with a resolution in the transverse momentum p_{T} of

about $\sim 1.5\,\%$. The tracker and calorimeter combine to provide good energy resolutioin for low as well as high momentum particles respectively.

At the LHC design luminocity of $10^{34}\ cm^{-2}s^{-1}$ there will be on average 1000 particles from roughly 23 overlapping proton-proton interactions traversing the tracker for each bunch crossing every 25 ns. A detector technology featuring high granularity and fast response is required such that the trajectories can be identified reliably and attributed to the correct bunch crossing. It is for this reason that the CMS tracker opted for silicon technology. Since silicon sensors are highly suited to receive many particles in a small space due to their fast response and spatial resolution. The tracker is tasked along with the ECAL and muon chambers to identify electrons and muons. Tracking information is also heavily used in the High Level Trigger (HLT) system of the CMS to reduce the event rate from the LHC bunch crossing rate of 40 MHz to about 100 Hz which can be permanently stored. One of the most important goals of the tracker is to minimize the effects on the tracking performance of electron bremsstrahlung and hadronic interactions. For this, the tracker has a track isolation criteria for identifying photons and electrons from electromagnetic clusters. This criteria is applied to suppress $\gamma - \pi^o(jet)$ and $\pi^o - \pi^o(jet - jet)$ backgrounds to a level significantly below the irriducible $\gamma - \gamma$ background.
The CMS tracker achieves this performance by using silicon pixel and strip trackers. It has about 1440 pixel and 15148 strip detector modules. The pixel tracker has 3 layers positioned at radii between 4.4 cm and 10.2 cm while the silicon strip tracker has 10 layers surrounding the pixel detector in the barrel and extending out ward to a radius of 1.1 m. Each system is completed by endcaps which consist of 2 disks in the pixel detector and 3 plus 9 disks in the strip tracker on each side of the barrel extending the acceptance of the tracker to a pseudorapidity of $|\eta| < 2.5$. The pixel detector also covers a pseudorapidity of $-2.5 < \eta < 2.5$ matching the acceptance of the central tracker. It is closest to the beam line directly surrounding the interaction vertex and has pixels of size $\approx 100 \times 150\ \mu m^2$ covering a total area of $\approx 1\ m^2$. The main function of the pixel detector is to provide precise tracking points in the $r - \phi$ and Z responsible for small impact parameter resolution of about $\sim 15\ \mu m$ [13],which is important for good secondary vertex reconstruction and position resolution. This is crucial in the identification of displaced vertex physics objects with life-time of about $\tau \approx 10^{-12}\ s$. They include particles such as $B^{0,\pm}$, $D^{0,\pm}$, $\tau^{\pm}$, which may travel a distinguishable distance ($c\tau \approx 100\ \mu$m.) before decaying into particles with tracks like electrons and muons. In addition, it is also important for forming seed tracks for outer track reconstruction and high level triggering.
The silicon strip detector covers the radii region 20 cm$< r <$ 110 cm. The over 15,000 silicon modules occupy an active area of 200 m^2 providing a coverage in pseudorapidity up to $|\eta| < 2.5$. It is also known as the outer tracker and consist of almost 9.6 million silicon strips providing a spatial resolution measured to be about 10 μm for $r - \phi$ measurement and about 20 μm for Z measurment necessary for particle trajectory reconstruction. At the intermediate radii (20 cm$< r <$ 55 cm), where the particle flux is reduced, it is instrumented with silicon micro strip in the barrel detector with a typical cell size of 10 $cm \times 80\ cm$ in $r - \phi$ and Z plane. The silicon modules here have sensors of thickness about 320 μm, while for radial distances; 55 cm$< r <$ 110 cm, the strip detector uses longer strips. The strip electric noise scales linearly with its length. Thus in order to maintain a good signal to noise ratio well above 10, the CMS uses thicker silicon sensors of about 500 μm which has correspondingly higher signal. Overal the Strip detector is made of 4 subdetectors. The Inner Barrel (TIB) consists of 4 cylindrical layers while the outer barrel (TOB) has 6 cylindrical layers. Two endcap detectors(TEC) in the positive and negative side of the Z cordinate consist of 9 carbon fiber disks with petal structure providing support for the modules. Signals from modules of both strip and pixel dectors are amplified by 4 to 6 Analogue Pipeline Voltage(APV25) read out chips mounted on the front-end hybrid(FE-hybrid). The hybrid provide key information such as temperature of the chips and timing information in order to match the recorded "hits" with collision.

3 Analysis Strategy

Neutralino decay would manifest itself as a topological signature where a very energetic photon originates from a vertex displaced from the LHC beam line. This displaced point can range from a few milimeters within the ECAL volume to astronomical distances out side the detector. Infact, the decay length of neutralino as seen from equation (11) is of the order of :

$$\mathsf{L} \sim \frac{\mathrm{F}^2}{\tilde{m}^5} \tag{12}$$

Therefore, depending on the value of F and the mass of neutralino($\tilde{m}$), its decay can be an instantaneous (prompt), non-prompt as well as delayed. This analysis focuses on the search from non-prompt to delayed neutralino decay. As a result, we expect the CMS detector to be most sensitive to neutralino decay within the ECAL volume.

Neutralino production at the LHC is of primarily two sources. In the first scenario, neutralino emerges as an end product from some weakly conserving R-parity decay of a higher mass SUSY particle. This type of production mechanism is refered to as GMSB. Secondly, neutralino can also be directly produced from parton-parton interactions like gluon-gluon fusion or gluon-quark or quark-quark interaction.
The decay kinematics of neutralino into γ and $\tilde{G}$ for each production mechanism will be unique. In this analysis we use as benchmark for understanding its kinematics the GMSB-produced neutralino (We explore other neutralino production mechanisms). Assuming the nuetralino is produced with very little momentum (momentum sligthly bigger than its mass) such that it is a slowly moving particle and that it decays entirely within the ECAL volume, our signature candidate for its presence will be events with one or two displaced vertices within the CMS tracker volume and photons with high transverse momentum (p_{T}) and large missing transverse energy ($E_{\mathrm{T}}^{\mathrm{miss}}$). We believe that these high p_{T} photons, because of the supposed large decay length of the neutralino, will arrive late at the ECAL and since SM does not predict any high mass (mass $> 200\ GeV/c^2$) and long lifetime ($\tau > 2\ ns$) particles, this is definitely a background free search with our main background from misreconstructed photons and decays in flight. With this kind of background, we expect that simple cuts to reduce this background can include:

1. Cut on the decay length (using ECAL Timing).
2. Cut on the p_{T} of the photon and its tracker quality(if any).
3. Cut on the missing transverse energy ($E_{\mathrm{T}}^{\mathrm{miss}}$).
4. Other topological cuts relating to how isolated the photon might be as well as the total number of associated jets in the event.

To be precised, the cuts we intend to apply for each event are the following: On photons, we will expect an isolated photon with a $p_{\mathrm{T}} > 90\ GeV/c$ in the pseudorapidity region of $|\eta| < 2.5$ while on the gravitino, we use a $E_{\mathrm{T}}^{\mathrm{miss}} > 30\ GeV/c^2$ to reject SM background missing transverse energy sources as well as detector inefficiency and require the $E_{\mathrm{T}}^{\mathrm{miss}}$ calculation to be within the pseudorapidity of the tracker range $|\eta| < 2.5$ and across all other subdetectors. Most importantly, we expect events with | ECAL TIME | $> 2\ ns$ to reduce mostly SM background.

3.1 Luminosity and Data Selection

Physics processes beyond the standard model have very small cross section. Therefore, measuring an observable of BSM process provides an extra challeng but at the same time an excellent opportunity because these processes have not been well studied. We discuss in the following sections; the various factors important to our analysis.

3.1.1 Luminosity

Luminosity expresses the rate at which a certain interaction will occur during proton-proton collisions. It is proportional to the number of particles colliding and inversely proportional to the transverse size of the bunches at collision. Interaction in CMS is defined to be inelastic proton-proton collisions leading to significant energy deposition in the main parts of the detector. The luminosity depends on the number of properties. For two gaussian distribution proton beams colliding head on, the luminosity dependence can be summarized in the following equation:

$$\mathcal{L} = \frac{N_1 N_2 N_b}{4\pi\sigma_x\sigma_y} f_{\mathrm{rev}} \tag{13}$$

where N_1 and N_2 are the number of protons in bunch 1 and 2 respectively and N_b is the total number of bunches. $\mathrm{f}_{\mathrm{rev}}$ is the revolution frequency of each bunch. The important factor here is the spread in the bunches in the transverse direction, denoted here as σ_x and σ_y during collision which depends on the design of the collider. The LHC has been designed to run at instantaneous luminosity between $10^{28} cm^{-2} s^{-1}$ and $10^{34} cm^{-2} s^{-1}$ at a bunch crossing rate of 40.08 MHz. An orbit of the machine comprises of 3564 bunches with about 10^{11} protons per bunch, of which 2835 have real collisions when running at designed luminosities.
The typical cross section for a given physics process is related to the instantaneous luminosity through:

$$\mathrm{R} = \sigma \times \mathcal{L} \tag{14}$$

where R is the observed rate for a physics process with cross section σ and $\mathcal{L}$ is the instantaneous luminosity. The number of events observed from a given physics process is therefore given by R. The CMS recorded total integrated luminosity of $\mathrm{L} = 5.20 fb^{-1}$ [16]. This is a reasonable amount of data for us to begin expecting the presence of physics process with theoretical cross section within the picobarn and the femtobarn range.

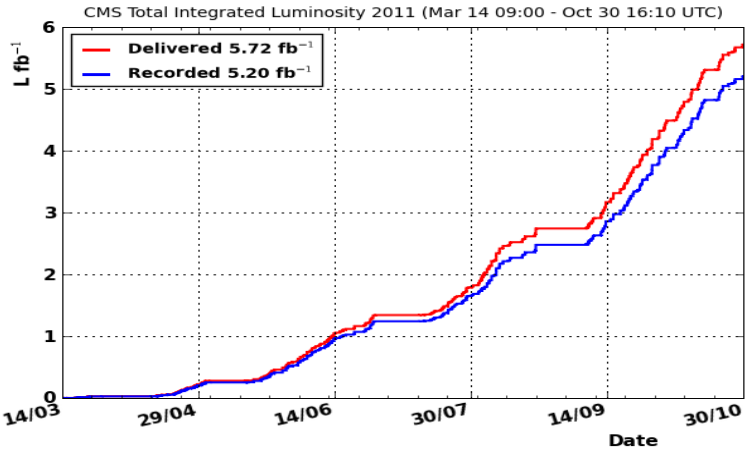

Figure 1: Total Integrated Luminosity vs Time delivered to (red), and recorded by CMS (blue) during stable beams for pp running at 7 TeV center-of-mass energy.

3.1.2 Data Selection

Data taking begins with the first level(L1) of the CMS trigger system, composed of custom hardware processors. Information from the calorimeter and muon system is used to select the most interesting events. The High Level Trigger(HLT) further decreases the event rate from around 100 KHz to 300 Hz, before data storage. This is very important as only very interesting physics events are stored for further event selection and there is no space or computer time to keep all the data. Event selection begins with triggering an interest event during data taking process. The advantage is that, processing time during analysis is reduced.

On-line Data Selection

The calorimeter trigger works on primitives from two sub-detectors: the electromagnetic calorimeter(to build electron and photon candidates) and the hadron calorimeter(which triggers jets.) Its main goal is to provide a list of the most energetic candidates from different classes, e.g $4e\gamma$,4μ, 4jets or MET(Missing Transverse Energy). The L1 trigger reduces the event rate from 40 MHz to 100 KHz. In figure 2, we give an example of the performance of an Level 1 ECAL electron trigger, which selects electrons with a threshold of 15 GeV. The efficiency is almost one after the threshold.

The High Level Trigger (HLT) code runs on large group of computers further decreases the event rate from around 100 KHz to around 300 Hz before data storage by analyzing a full event. It further subdivides the data into data streams with respect to physics. The data selection requirement normally includes the following: for a example, with a candidate photon, the selection criteria might include a high p_{T} isolated photon(to remove Jets faking photons), with p_{T} above a certain threshold(to remove events arising from soft collisions), within a given geometrical region of the calorimeter, usually the EB where energy resolution is best. Event selection sometimes require events originating from a given number of interaction vertices and with a given number of Jets associated with them. This kind of primitive selection also defines the off-line selection.
Event reconstruction uses a Particle-Flow(PF) algorithm. It consists reconstructing and identifying each particle with an optimized combination of all sub-detector information. The energy of a photon is directly obtained from the ECAL measurement, corrected for zero-suppression effects. The energy of neutral hadrons is obtained from the corresponding calibrated ECAL and HCAL energy. Figure 3 is an example of an HLT Photon trigger, selecting diphoton objects with a minimum transverse momentum of 32 GeV and 26 GeV. The efficiency reaches one beyond the 32 GeV threshold.

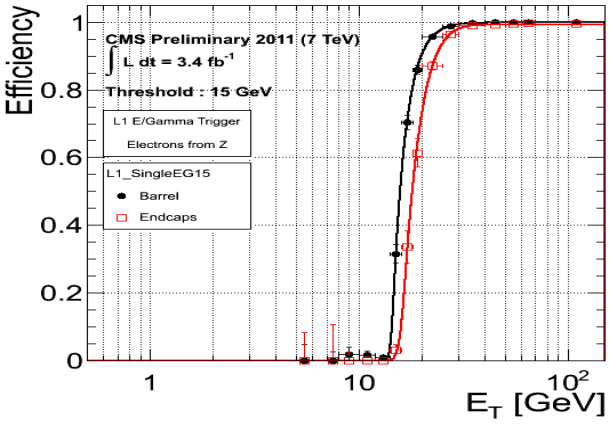

Figure 2: Efficiency of Level 1 ECAL Electron Trigger.

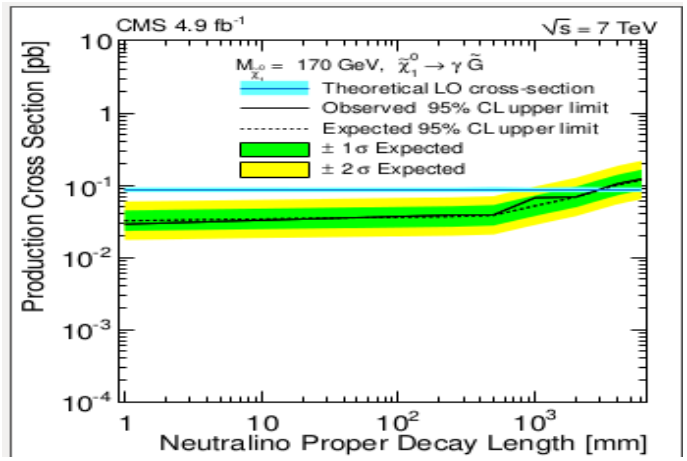

Figure 3: Efficiency for diphoton HLT Trigger.

3.2 Missing Transverse Energy($E_{\mathrm{T}}^{\mathrm{miss}}$) and Ecal Time Reconstruction

In a large signal parameter space, the $\tilde{\chi}_1^0$ has a non-neglible lifetime($\tau_{\tilde{\chi}_1^0}$). The decay into a delayed photon and a neutral gravitino prompts the use of Calorimeter timing and the missing transverse energy(MET) or $E_{\mathrm{T}}^{\mathrm{miss}}$ as background discriminating variables. The photon time is considered as the "cluster time" or in rare cases "the supercluster time" where a cluster is a collection of crystals and a super cluster is a collection of basic clusters. If the photon energy is spread on many clusters, then it is considered to be a super cluster and the time is calculated using the time of impact of the seed cluster (highest energy cluster) in the super cluster.

3.2.1 ECAL Time Reconstruction

Photons travel with the speed of light. Their time of travel from collision point to calorimeter crystals is taken as reference for any other physics object. From a detector point of view, each photon is seen as a cluster of energy hits on crystals. Therefore, a logical way to define the photon arrival time, is to find the average of the time measured by each crystal as:

$$T_\gamma \quad = \quad \sum_i^{N_{xtal}} \frac{T_{RECO,i}}{N_{xtal}} \tag{15}$$

where $i = 1, \cdots, N_{xtal}$ and N_{xtal} is the number of crystals in the cluster. where T_{RECO} is the reconstructed time such that avearging over number of events $\langle T_{RECO} \rangle \approx 0$. By definition, $T_{RECO,i} = T_{RAW,i} + Constant$. The constant consist of channel-to-channel inter calibration and any global phase shift. Finding new constants such that on average, $\langle T_{RECO} \rangle \approx \langle T_{RAW} \rangle \approx 0$ is called timing calibration. We obtain T_{RAW} from the reconstructed time T_{MAX}. In the following paragraph, we briefly describe the process of obtaining T_{MAX} from the reconstructed hits.

The signal develops when an energetic hit impinge on the crystal. The crystal, through a process of scintillation, convert the energy of the hit into light which propagate through the crystal as an electromagnetic shower to the end of the crystal where it is collected by photo detectors.The front end electronics amplify and shape the signal from the photo detectors. The pulse shape is defined by the analog part of the front end electronics. For each given channel(crystal), all particles result in the same pulse shape to a very good approximation. The pulse is digitized at 40 MHz by a voltage-sampling analog-to-digital converter on the front end, producing discrete samples of the amplitude as illustrated in Figure 4. Figure 4(a) shows the typical measured signal pulse in the ECAL after amplification(solid line). The amplitude of the pulse, A, is shown as a function of $T - T_{MAX}$. T is the time of ADC sample and T_{MAX} is defined as the time when the pulse reaches its maximum value A_{MAX}. These samples are stored in a buffer until a Level-1 trigger is received, prompting the transmission of ten consecutive samples to the off-detector electronics for insertion into the CMS data stream.
We define the ECAL time reconstruction as the measurement of T_{MAX} using the ten available samples of the pulse amplitude. Similarly, ECAL energy reconstruction is defined as the determination of the true pulse amplitude, A_{MAX} [17]. For each channel, the values of the pulse samples depend on three factors: The value of A_{MAX}; the relative position of T_{MAX} between time samples, which will be referred to as a "T_{MAX} phase", and the pulse shape

itself.
A very good alternative often used to represent the pulse shape as *A(T)*, is the ratio variable, defined as $R(T) = \frac{A(T)}{A(T+25ns)}$. This has advantage that any systematic errors cancel out. Figure 4(b) shows the measured pulse shape using variables $T - T_{MAX}$ *vs R(T)*. This pulse representation, *T(R)*, is independent of A_{MAX} (albeit not so true with very low and very high amplitude hits). It can be described very well with a simple polynomial parametrization *T(R)* as seen in Figure 1(b). A pair of consecutive samples give a direct measurement of the ratio $R_i = \frac{A_i}{A_{i+1}}$ and thus a measurement for each sample of $T_{MAX,i} = T_i - T(R_i)$. The uncertainty on each time measurement for each sample, σ_i, is given as a product of the derivative of the *T(R)* function and the uncertainty on the value R_i, where i is the i^{th} ratio. Ratios with large derivative of *T(R)* and $A \approx 0$ are not used, since this is quite closed to the pedestal value. This uncertainty in R_i has three independent contributions which are added in quadrature. The first one is due to noise fluctuations, σ_n, in each sample. The second contribution is due to the uncertainty in the estimation of pedestal value which is subtracted from the measured amplitude in each sample. The last contribution is due to truncation during 12-bit digitization.

Typically, there are four or five ratios available per pulse. The reconstructed time of the hit and its errors are determined using the formula for the weighted average, assuming that the ratios are uncorrelated:

$$\mathsf{T_{MAX}} = \frac{\sum \frac{T_{MAX,i}}{\sigma_i^2}}{\sum \frac{1}{\sigma_i^2}} \tag{16}$$

;

$$\frac{1}{\sigma_{\mathsf{T}}^2} = \sum \frac{1}{\sigma_i^2}. \tag{17}$$

This formula despite its success in medium energy hits, performs poorly with very low (< 2 GeV) and very high energy(> 100 GeV) hits. We are currently working on improving this. Nevertheless, the good thing about this method is that it is less affected by the "T_{MAX} phase" than the normal represenation method of figure 1(a). Using this algorithm, the time resolution is shown to be less than 400-500 ps [1] for energy deposits larger than 10-20 GeV in the barrel.
To be able to evaluate this performance, consider a decay path length of 10 cm for a long-lived particle. The ECAL time measurement would equate around 334 ps. This is considerable not very far from a typical in-time measurement for an in-time photon. Indeed for the most energetic ECAL crystal with energy 10 $GeV < E < 100$ GeV, within the barrel region ($|\eta| < 1.479$), the time resolution is about $400 - 500$ ps, we can still argue that the ECAL time is a very powerful variable for identifying displaced photons.

3.2.2 $E_{\mathrm{T}}^{\mathbf{miss}}$

Missing energy is the apparent signal of neutrinos or some weakly interacting stable particles in a detector. Modern detectors at hadron colliders are designed to provide close to 4π coverage in solid angle with calorimetry. The CMS detector provides this hermicity with the ECAL and HCAL to calculate missing energy.
In a hadron collider like the LHC, it is quite challanging to know with very good approximation; along the longitudinal direction of the beam pipe, the total energy of the colliding partons making up the protons. As a result, energetic particles produced in the direction of the beam pipe makes it almost impossible to directly measure the energy imbalance (missing energy) parallel to the beam direction. On the other hand, since the colliding partons are travelling with very high forward momentum or momentum parallel to the beam line, it is logical to assume that on the plane transverse to the beam pipe just before impact, their total momentum on this plane is zero. Knowing that the initial transverse momentum is zero, the final(after impact) transverse momentum can be measured to a good approximation such that the transverse energy imbalance defined as the magnitude of the total transverse momentum imbalance measured is good enough to help establish a physics signature involving one or more non-interacting particles.
With this assumption that the total transverse momentum of the partons in the proton just before collision is very minimal or zero and using conservation of transverse momentum (momentum transverse to the beam pipe), the total sum of the transverse momentum of all the particles produced after collision must also equal zero. After carefully measuring the transverse momentum for all the particles which deposited energy in the calorimeter and left tracks in the tracker as they interacted with the detector, the transverse momentum imbalance is considered

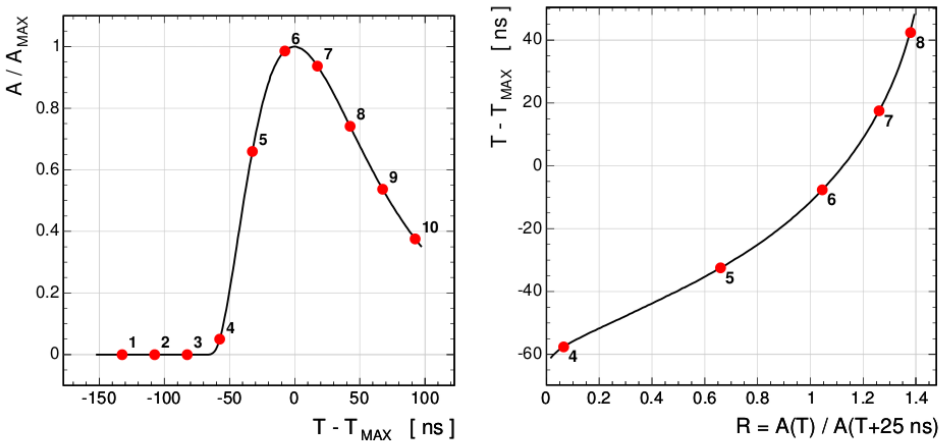

Figure 4: Left: Typical measured ECAL pulse shape. The *x-axis* represents the distance between the position of the ADC sample (T) from the expected maximum of the pulse shape (T_{MAX}) while the *y-axis* shows the amplitude in each sample normalized to the maximum. Right: $T - T_{MAX}$ as a function of the value of the measured ratio of the amplitude in two consecutive samples (R). The solid line is the average pulse shape as measured with an synchronous beam of electrons. The dots indicate ten discrete samples of the pulse, corresponding to a single event.

as the momentum or energy carried away by the weakly-interacting particles produced. This transverse momentum imbalance is also called the missing transverse momentum vector $E_{\mathrm{T}}^{\mathbf{miss}}$. $E_{\mathrm{T}}^{\mathrm{miss}}$ is considered as the physics signature for energetic neutrinos or other weakly interacting stable particles. The discovery of the W in the decay $\mathrm{W} \to \ell\nu$ used $E_{\mathrm{T}}^{\mathrm{miss}}$. The electron is observed as an energy deposit in the ECAL with a track in the tracker while the neutrino is identified by the $E_{\mathrm{T}}^{\mathrm{miss}}$ calculated event-by-event. Missing transverse energy corrections arising from detector inefficiency is extracted in the low $E_{\mathrm{T}}^{\mathrm{miss}}$ region by measuring the transverse mass of W and Z to be applied in the measurement of high $E_{\mathrm{T}}^{\mathrm{miss}}$ where the measurement is not very reliable. The purpose of this is to improve the mearsurement of high $E_{\mathrm{T}}^{\mathrm{miss}}$.
The belief that other new particles produced at the hadron collider will express themselves through $E_{\mathrm{T}}^{\mathrm{miss}}$ has led to deligent studies of $E_{\mathrm{T}}^{\mathrm{miss}}$ in terms of identifying other sources of $E_{\mathrm{T}}^{\mathrm{miss}}$ which may not be real and could result from the many inherent detector inefficiency.

Reconstruction of missing transverse energy vector; $\vec{E}_{\mathrm{T}}^{\mathrm{miss}}$ involves ECAL and HCAL cells combined to form calorimeter towers with the η and φ of the tower segmentation defined to match the granularity of the hadron calorimeter or HCAL geometry. $\vec{E}_{\mathrm{T}}^{\mathrm{miss}}$ is calculated by summing individual calorimeter towers having energy E_n and pseudorapidity η_n and azimuthal angle φ_n as:

$$\vec{E}_{\mathrm{T}}^{\mathrm{miss}} = -\sum_n \left(\frac{E_n \cos\varphi_n}{\cosh\eta_n}\hat{x} + \frac{E_n \sin\varphi_n}{\cosh\eta_n}\hat{y} \right) = E_x^{Miss}\hat{x} + E_y^{Miss}\hat{y} \tag{18}$$

Physics objects like muons which deposit very small amount of energy in the calorimeter(about 4 GeV) are taken into account and their calorimeter energy deposit replaced with their reconstructed track p_{T}.
Other possible sources of miss measured $E_{\mathrm{T}}^{\mathrm{miss}}$ include: Noise in the HCAL, cosmic muons traversing the detector, beam halo, cracks in the detector as well as misidentification of physics objects in the reconstruction of the total transverse energy. Despite all these challenges in $E_{\mathrm{T}}^{\mathrm{miss}}$ calculation, better and smarter algorithms have been developed which take into consideration all these sources of fake $E_{\mathrm{T}}^{\mathrm{miss}}$. A very good algorithm which is very reliable is the (PF) $E_{\mathrm{T}}^{\mathrm{miss}}$ algorithm which is a common tool for calculating $E_{\mathrm{T}}^{\mathrm{miss}}$. It uses charged track corrections where p_{T} measurement from the tracker replaces their corresponding ECAL energy. Removal of fake sources of $E_{\mathrm{T}}^{\mathrm{miss}}$ like noise from HCAL can be done by requiring a certain minimum p_{T} threshold on an isolated physics object from a properly identified Primary Vertex(PV) as it is done here [19] and here [20]. Figure 5(a) below shows the distribution of a simulation and data of $E_{\mathrm{T}}^{\mathrm{miss}}$ in dijet events using the PF algorithm. While Figure 5(b) shows the $E_{\mathrm{T}}^{\mathrm{miss}}$ distribution for a simulated neutralino decay into photon and gravitino as well as $E_{\mathrm{T}}^{\mathrm{miss}}$ from background(photon dataset) for different jet multiplicities in an Event.

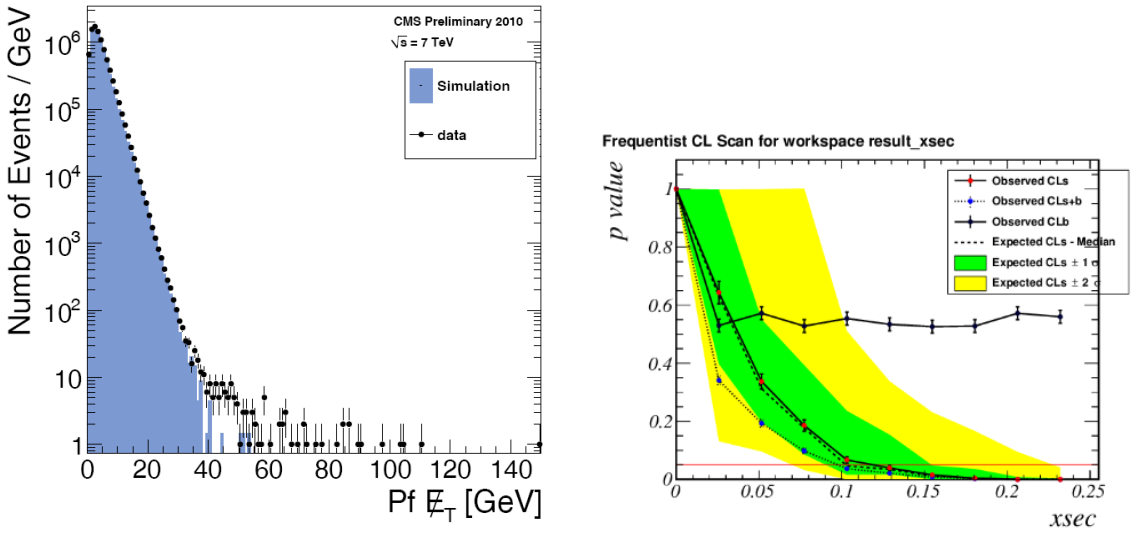

Figure 5: (a)PF MET for inclusive dijet events distribution. (b) PF MET for events with simulated neutralino decay into photon and gravitino with proper life-time of neutralino $c\tau = 250\ mm$(grey color) and background(data) QCD photons from events with at least 3Jets(blue) and at most 2 Jets(pink). The plots in (b) have been normalized to unity.

In an environment like the LHC, with multiple pp collision per beam crossing, including soft-collisions which give rise to pile-up events; this makes calculation of $E_{\mathrm{T}}^{\mathrm{miss}}$ vector even more challenging. These low p_{T} events degrade the energy resolution of the detector especially the calorimeter energy resolution which is the dorminant contribution to poor $E_{\mathrm{T}}^{\mathrm{miss}}$ resolution in CMS. The is progress in this direction to use particle-flow(PF) techniques for measuring individual p_{T} of the reconstructed physics object contributing to the total transverse energy.
Anomalous signals in ECAL and HCAL give rise to anomalous energy deposits due to some bad channels. In a situation where a group of ECAL and HCAL channels are bad, the only remedy is to mask out affected channels contributing to $E_{\mathrm{T}}^{\mathrm{miss}}$ reconstruction. This process is refered to as $E_{\mathrm{T}}^{\mathrm{miss}}$ "*cleaning*". If a large number of channels is affected, then that particular dataset is not used for physics analysis. An example where the performance of $E_{\mathrm{T}}^{\mathrm{miss}}$ is studied, is in events that contain genuine $E_{\mathrm{T}}^{\mathrm{miss}}$ like $\mathrm{W} \to \ell\nu$, where ℓ is a muon or electron and ν is identified through $E_{\mathrm{T}}^{\mathrm{miss}}$.
Excellent simulation of high $E_{\mathrm{T}}^{\mathrm{miss}}$ using monte-carlo still remains one of the major challenges in the reconstruction of $E_{\mathrm{T}}^{\mathrm{miss}}$ for CMS.

3.3 Current and Future Work

Our current and future work is directed in two fronts.

ECAL Timing: Improving on the ECAL timing resolution for mostly high energy photons(E > 100 GeV) remains an important task. As a good and reliable timing calibration is crucial for background rejection effeciency studies from mostly prompts events from SM model interactions.
We introduce new definition for photon candidate timing such as:

1. Weighted average of T_{RECO} over the number of channels in cluster; each weight is the error per channel.
2. Time of the most energetic reconstructed hit(seed crystal) of the crystal in the cluster.

to improving on the timing measurement.

MET: New $E_{\mathrm{T}}^{\mathrm{miss}}$ reconstruction algorithm with variables like E_{T}^{miss} *significance* ($E_{\mathrm{T}}^{\mathrm{miss}}$ S) [22] could be used to quantify the significance in $E_{\mathrm{T}}^{\mathrm{miss}}$ reconstruction by evaluating the uncertainty in the total measured transverse momentum, given by

$$\vec{E_{\mathrm{T}}^{\mathrm{miss}}}^{total} = -\sum_{i \in X} \vec{E_{\mathrm{T}i}} \tag{19}$$

where $\vec{E}_{\mathrm{T}i} = (E_{x_i}, E_{y_i})$ is the measured transverse momentum of the i^{th} reconstructed object. X is the set of reconstructed objects, such as calorimeter towers (for Calo $E_{\mathrm{T}}^{\mathrm{miss}}$) or PF particles (for PF $E_{\mathrm{T}}^{\mathrm{miss}}$), used to calculate the $E_{\mathrm{T}}^{\mathrm{miss}}$. A detailed account of this is found in [22].

4 Conclusion

We have presented a proposal of an analysis to search for GMSB particles using displaced photons and outlined in detail our candidate strategy for the search.
In section 1, we began by introducing GMSB models, stating some of the general and especially theoretical motivations for the choice of these super-symmetry models. In Section 2, we give a description of the CMS detector at LHC, stating very important aspects of using this detector in GMSB searches. In section 3, we outline a possible analysis procedure mentioning some of the relevant variables we will consider with detailed description and physics motivated arguments. In the coming years, with improved detector understanding and performance, these variables will be very reliable in discriminating background from signal with better efficiency and significance.

References

[1] CMS Collaboration, "Time Reconstruction and Performance of the CMS Crystal Electromagnetic Calorimeter",CFT-09-006, 2009.

[2] J.Ellis, J.Hagelin, D. Nanopoulos, K.A. Olive and M. Srednicki; *Nucl. Phys.* B238 (1984) 453; H. Goldberg, *Phys. Rev. Lett* 50 (1983) 1419; J. Ellis, T. Falk, G. Ganis, K.A. Olive and M. Srednicki, *Phys. Lett.* B 510 (2001) 236, arXiv: hep-ph/0102098.

[3] G.F. Giudice and R. Rattazzi "Theories with Gauge-Mediated Supersymmetry Breaking" arXiv:hep-ph/9801271v2

[4] H. N. Brown et al., Muon $g_\mu - 2$ Collaboration, *Phys. Rev. Lett* 88 (2002) 2227, hep-ex/0102017; A. Czarnecki and W.J. Marciano, *Phys. Rev.* D 64 (2001) 013014, hep-ph/0102122.

[5] M. Knecht and A. Nyffeler, hep-ph/0111058; I. Blokland, A. Czarnecki and K. Melnikov *Phys.Rev. Lett* 88 (2002) 071803 hep-ph/0112117

[6] CLEO Collaboration, M. S Alan et al., *Phys. Rev. Lett.* 74 (1995) 2885 as updated in S. Amed et al., CLEO CONF 99-10; BELLE Collaboration hep-ex/0103042

[7] S.Mathin, arXiv:hep-ph/9709356

[8] B.Allanach et al,arXiv:hep-ph/0202233v1

[9] J.Dann et al.(LEPSUSY Working Group), Internal note LEPSUSYWG/97-04(1997), P. Janot, talk at the EPS Conference, Jerusalem, 1997.

[10] CDF Collaboration, "Search for Supersymmetry with Gauge-Mediated Breaking in Diphoton Events with Missing Transverse Energy at CDFII ",*Phys. Rev. Lett.*

[11] ATLAS Collaboration "Search for Diphoton Events with Large Missing Transverse Momentum in 1 fb^{-1} of 7TeV Proton-Proton Collision Data with the ATLAS Detector", arXiv:1111.4116v1,17th Nov 2011.

[12] CMS Draft Analysis,"Search for Long-Lived Particles using Displaced Photons in PP Collision at $\sqrt{S} = 7TeV$ ", CMS AN AN-11-081 **104(2010)011801,**

[13] CMS Collaboration,"CMS Physics: Technical design report, Volume 1" CERN-LHCC-2006-001

[14] CMS uses a right-handed coordinate system, with the origin at the nominal interaction point, the $\boldsymbol{x}$-axis pointing to the center of the LHC, the $\boldsymbol{y}$-axis pointing up (perpendicular to the LHC plane), and the $\boldsymbol{z}$-axis along the counterclockwise-beam direction. The polar angle, $\boldsymbol{\theta}$, is measured from the positive $\boldsymbol{z}$-axis and the azimuthal angle, $\boldsymbol{\phi}$, is measured in the $\boldsymbol{x}$-$\boldsymbol{y}$ plane. $\boldsymbol{\eta = -\ln\tan(\theta/2)}$. The transverse energy and momentum are defined as $\boldsymbol{E_T = E\sin\theta}$ and $\boldsymbol{p_T = p\sin\theta}$ where E is the energy measured in the tracking system.$\boldsymbol{E_T^{miss} = |-\sum_i E_T^i \vec{n}_i|}$ where $\boldsymbol{\vec{n}_i}$ is a unit vector that points from the interaction vertex to the transverse plane.

[15] CMS Collaboration, "The CMS experiment at the CERN LHC", JINST 0803:S08004, 2008.

[16] CMS Collaboration,"CMS trigger and data taking in 2010*",CMS CR-2011/051.

[17] CMS Electromagnetic Calorimeter Collaboration, "Reconstruction of the signal amplitude of the CMS electromagnetic Calorimeter", Eur.Phys.J.C46S1(2006)23-35.

[18] D.del Re et al "An algorithm for the determination of the flight path of long-lived particles decaying into photons" CMS AN -2010/212.

[19] CMS Collaboration,"Particle-Flow Event Reconstruction in CMS and Performance for Jets, taus and $\not\!\!E_{\mathbf{T}}$", CMS Physics Analysis Summary CMS-PAS-PFT-09-001(2009).

[20] CMS Collaboration, Missing Transverse Energy Performance in Minimum-Bias and Jet Events from Proton-Proton Collisions at $\sqrt{s} = 7$ TeV , CMS Physics Analysis Summary CMS-PAS-JME-10-004 (2010).

[21] MET JINST (arXiv:1106.5048)

[22] CMS Collaboration, "Missing transverse energy performance of the CMS detector"; arXiv:1106.5048v1

[23] CMS Collaboration,"CMS Physics: Technical design report, Volume 2" CERN-LHCC-2006-001.

[24] CMS Electromagnetic Calorimeter Collaboration, "Energy resolution of the barrel of the CMS Electromagnetic Calorimeter",JINST 2(2007)P04004.

[25] CMS Collaboration,"The electromagnetic calorimeter. Technical design report ",. CERN-LHCC-97-33